Using different atmospheric correction methods to classify remotely sensed data to detect liquefaction of the February 2011 earthquake in Christchurch

Amelie Broszeit[1], Salman Ashraf[2]

[1]Department of Remote Sensing
Julius-Maximilians University Würzburg. Würzburg, Germany
Phone: +49 17699092454
Email: ameliebroszeit@gmx.de

[2]Regional Geology Department
GNS Science, Lower Hutt, New Zealand
Phone: 04 5704624 Fax: 04 5701444
Email: s.ashraf@gns.cri.nz

Presented at SIRC NZ 2013 – GIS and Remote Sensing Research Conference
University of Otago, Dunedin, New Zealand
August 29th – 30th 2013

***Keywords and phrases*:** RapidEye, GeoEye-1, aerial image, Christchurch earthquake 2011, COST reflectance correction, ATCOR-2, supervised classification, Minimum Distance Classification, remote sensing, satellite imagery

1.0 INTRODUCTION

The 2010 - 2012 Canterbury earthquake sequence caused widespread damage. Much of the damage to residential buildings and infrastructure in and around Christchurch city was caused by permanent ground damage including liquefaction.

Remote sensing imagery provides information across a spatially widespread area to assess damage distribution following natural disasters. Satellite images (from the RapidEye and GeoEye-1 sensors) and aerial imagery, captured shortly after the February 2011 earthquake, showed liquefaction damage occurred over large areas of the Canterbury region.

This paper's main objective is to use different reflectance correction algorithms and test which provides the best results for classifying liquefaction. The study compares two reflectance correction models; the cosine of the solar zenith angle (COST) model (Chavez, 1996) and the atmospheric and terrain correction (ATCOR2) model (Richter, 1996) which calculates ground reflectance for a flat surface. The ATCOR2 model uses MODTRAN (moderate resolution atmospheric transmission) radiative transfer code (Berk et al. 1998) to calculate a broad range of predefined atmospheric correction functions stored as look-up tables (Richter, 1997). This is followed by a comparison of the results computed from supervised classification of images that were derived from different reflectance correction methods on RapidEye and GeoEye-1 imageries.

Atmospheric correction is an important processing step that removes time- and scene-dependent effects from remotely sensed data (Mahiny & Turner, 2007) and extracts quantitative information accurately (Liang, 2001). Many studies (Gebreslasie et al., 2009; Mahiny & Turner, 2007; Wu et al., 2005) have made comparisons between different atmospheric correction methods that demonstrate the significance of atmospheric correction for improved vegetation classification and change detection from remotely sensed data. Remote sensing images have been widely used to detect Earthquake damages. Mitomi et al. (2002), Oommen et al. (2010), Ramakrishnan et al. (2006) and Yusuf et al. (2001) have worked on detecting liquefaction using medium resolution aerial and satellite images; however, the effect of atmospheric correction to improve liquefaction detection is not well established.

2.0 MATERIALS AND STUDY AREA

Images from RapidEye and GeoEye-1 satellites and from a digital camera were taken shortly after the February earthquake. The RapidEye image, which was taken on the 24th of February 2011, has a 5 meter spatial resolution in 5 spectral bands. The GeoEye-1 image was taken on the 27th of February 2011 and has a spatial resolution of 1.65 meters in 4 spectral bands. The colour infrared (CIR) aerial image was taken on the 24th of February 2011 and has a spatial resolution of 0.5 meters in 4 spectral bands. All three images cover a large area over the Canterbury region, from 43° 29' 46.83" S and 172° 39' 40.07" E in the north to 43° 31' 38.51" S and 172° 39' 41.62" E in the south. The study area is located in the Avonside-Richmond area in 1-2 km north of Christchurch city (see Figure 1).

The earthquake happened on the 22th of February 2011 reaching a magnitude of 6.2 on the Richter scale. In the Avonside-Richmond area, liquefaction was widespread, on meadow areas as well as on streets and parking lots (see Figure 1). The three different images show the same area in three different spatial resolutions.

(a) (b) (c)

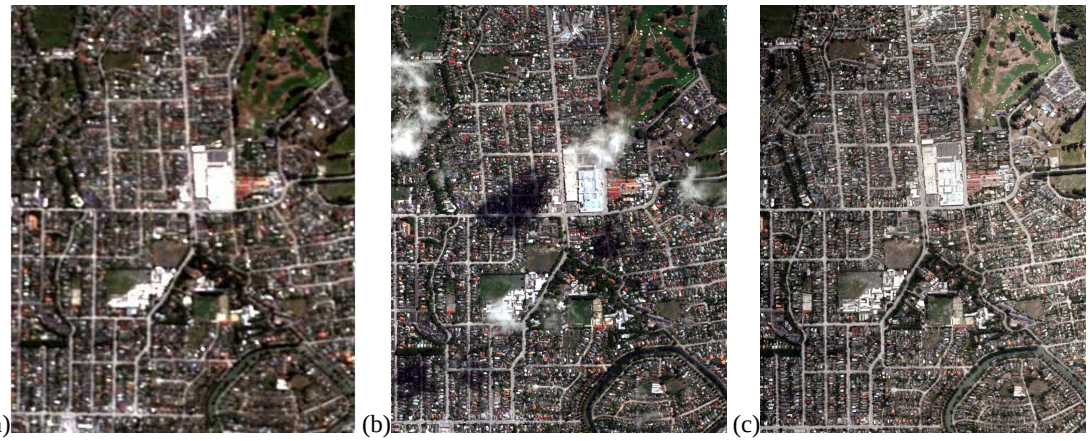

Figure 1: *(a) true colour RapidEye (5 m resolution), (b) true colour GeoEye-1 (1.65 m resolution), (c) true colour aerial photo (0.5 m resolution)*

3.0 DATA PROCESSING

The data processing shown in figure 2 has been applied on these images.

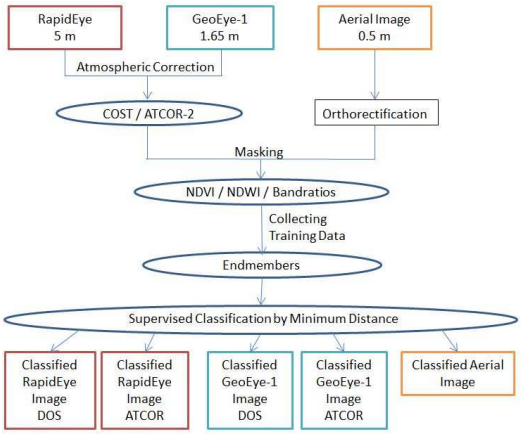

Figure 2: *Flow chart of the data processing*

3.1 Pre-Processing

On both satellite images, two different reflectance correction models were applied. The COST model converted image pixels first into the Top-of-Atmosphere (ToA) radiance and from there into the ToA reflectance using information from the metadata of these images. A fixed value of 1% of ToA radiance was used as the path radiance to remove the haze from these images (Chavez, 1988). The ATCOR method used a radiative transfer calculation based on the MODTRAN 5 code.

Figure 3 and 4 show examples of the spectral response showing the average of 15 random pixels in the RapidEye and GeoEye-1 image using the COST and ATCOR method. The (a) profiles show that the spectral profiles are similar for vegetation but in the (b) profiles, the spectral profiles for liquefaction show the COST method values to be higher than the ATCOR values.

After the conversion to reflectance, the Normalized Difference Vegetation Index (NDVI) and the Normalized Difference Water Index (NDWI) were calculated to remove potentially non-liquefaction pixels from the data. After masking out vegetation and water pixels, different band ratios were applied to remove as many pixels as possible to achieve an image which contains pixels having a spectral profile similar to the spectral profile of liquefaction as shown in figures 3 (b) and 4 (b).

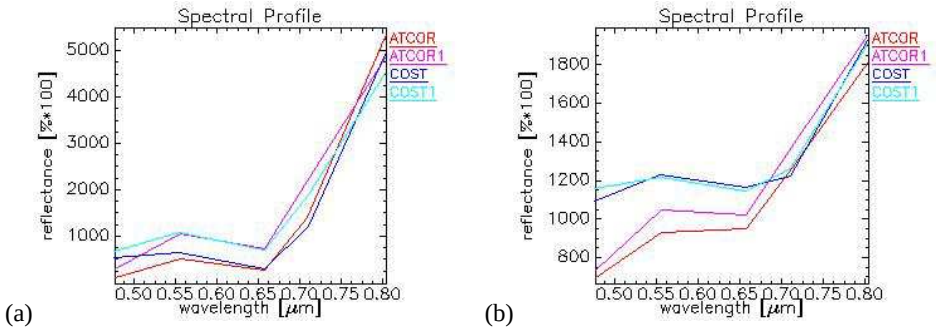

Figure 3: *RapidEye mean spectral profiles of (a) vegetation and of (b) liquefaction.*

Figure 4 shows examples of the results in the GeoEye-1 image using COST and ATCOR methods.

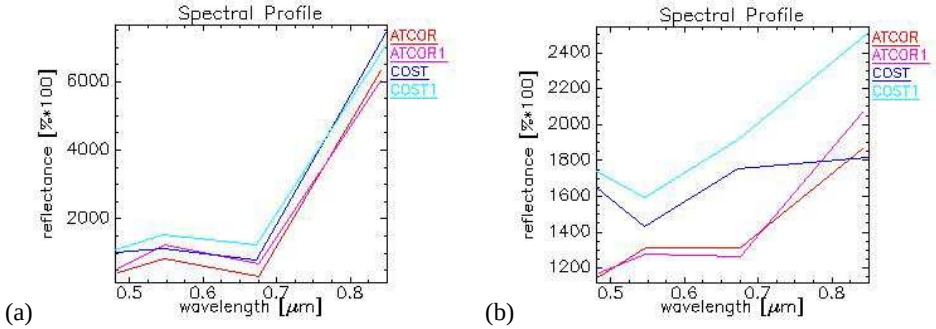

Figure 4: *GeoEye-1 mean spectral profile of (a) vegetation and of (b) liquefaction*

3.2 Classification of RapidEye, GeoEye-1 and Aerial Data

The classification of liquefaction is done by using the Minimum Distance supervised classification algorithm. The collected endmember spectra (consisting of about 15 pixels or more) such as different types of liquefaction as well as different urban types which are still left in the image were digitised directly from the image by hand digitising. These spectra were used as input for the classification. The resulting classes were manipulated using ENVI's n-D Visualizer tool.

4.0 RESULTS

The Minimum Distance classification method was tested on the COST and ATCOR reflectance RapidEye images, the ATCOR reflectance GeoEye-1 image and the aerial image. Classification has not applied on the COST reflectance GeoEye-1 image for this study; this is because a fixed value used to correct the atmospheric scattered path radiance (haze) from each band of this particular image (due to the presence of cloud) showed inconsistent spectral signatures for the liquefaction profile when compared with the ATCOR data (see Figure 4 (b)). The classification results from all images were then compared for accuracy.

The supervised classification accuracies are presented in table 1. Field data recently collected for the liquefaction mapping were available to test the accuracy of image classification (Brackley, 2012). Comparison of the overall accuracy of the three images, computed from RapidEye and GeoEye-1 reflectance images as well as from the

aerial image, show that the ATCOR model applied on the RapidEye image shows the best Overall Accuracy with 72.47 %.

Table 1: *Comparative data of supervised classification accuracies for all three images*

Classified Images	**RapidEye**		**GeoEye-1**	**CIR Aerial Image**
	ATCOR	COST	ATCOR	
Producer's Accuracy (%)				
Liquefaction	82.02	72.50	61.84	33.00
No Liquefaction	62.92	52.50	55.26	66.00
User's Accuracy (%)				
Liquefaction	68.87	60.42	58.02	49.25
No Liquefaction	77.78	65.63	59.15	59.62
Overall Accuracy (%)	**72.47**	**62.50**	**58.55**	**49.50**

There were similar reflectance signatures between liquefaction areas and some roofs and concrete surfaces. As a result there was partial success in eliminating non-liquefaction pixels from the data. Higher overall classification accuracies of RapidEye data were due to its higher spectral resolution, whereas higher spatial resolution images (GeoEye-1 and aerial) show lower classification success as there are more pixels having similar reflectance between liquefaction areas and roof/concrete surfaces. The figures 5-7 show the classification results of the same area at different spatial resolutions.

In figure 5, the classification on the ATCOR reflectance image shows the area of liquefaction more accurately than the classification on the COST reflectance image, as there is a better distinction between liquefaction and non-liquefaction areas.

(a)  (b) 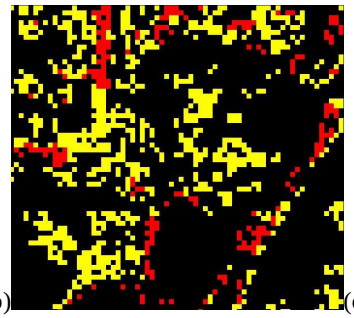 (c) 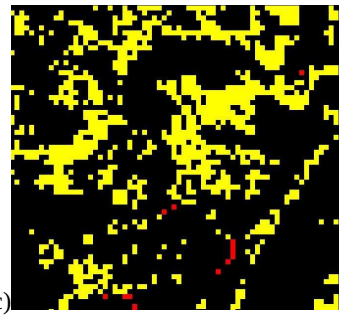

Figure 5: *(a) true colour RapidEye image, liquefaction is shown by the grey colour in the centre right of the image, (b) Minimum Distance classification after ATCOR reflectance correction, (c) Minimum Distance classification after COST reflectance correction (yellow: liquefaction, red: roof/concrete surfaces)*

The classification on GeoEye-1 ATCOR reflectance image in figure 6 (b) shows the liquefaction class less accurate compared to the RapidEye image. It is due to its low spectral resolution which leads to difficulties in classifying liquefaction and non-liquefaction pixels.

(a)  (b) 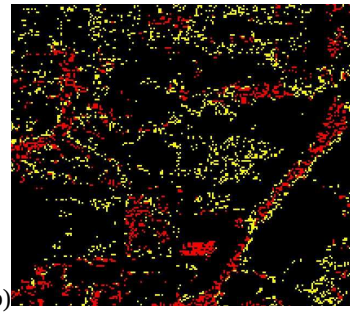

Figure 6: *(a) true colour GeoEye-1 image, (b) Minimum Distance classification after ATCOR reflectance correction (yellow: liquefaction, red: street, buildings).*

The classification of the CIR aerial image in figure 7 resolves liquefaction areas with more details compared to satellite images; this is because during the pre-processing fewer pixels were masked out thus leave behind many materials (such as roofs and roads) classified as liquefaction. This causes the low Overall Accuracy of 49.5 % (see Table 1) for the classification applied on the aerial image.

(a)  (b) 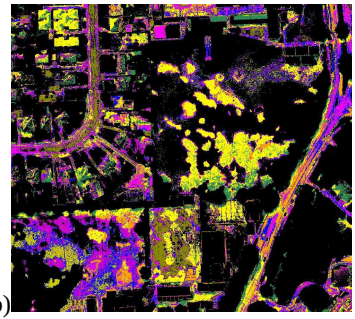

Figure 7: *(a) true colour CIR aerial image, (b) Minimum Distance classification (yellow: liquefaction, magenta: concrete, sea green: embankment, blue: grey roof)*

The classification applied on the COST reflectance corrected image shows lower overall accuracy than the classification applied on the ATCOR reflectance corrected images. This is because the COST method selected the lowest pixel values of each band automatically to remove the atmospheric haze from the data. The ATCOR method uses specific atmospheric and sensor geometry parameters to achieve a better reflectance conversion compared to the COST method.

5.0 CONCLUSIONS

The study used two different reflectance algorithms applied on data with different spatial and spectral resolution to detect and classify liquefaction.

The Minimum Distance classification applied on the RapidEye ATCOR reflectance corrected image shows the highest Overall Accuracy with 72.47 %. The ATCOR method results proved more accurate than the COST method.

The results show that it is difficult to get a precise classification of liquefaction in urban areas. The classification fails to distinguish in many places between liquefaction, roofs and concrete surfaces. As compared to previous studies (Oommen et al. and Ramakrishnan et al.), a low spectral resolution (i.e. lack of shortwave infrared band) of these images is also a limiting factor in detecting soil moisture/liquefaction.

A possibility to improve the results would be to use LIDAR data to eliminate building structures. Further processing using object-based classification is another option to improve classification accuracy.

ACKNOWLEDGEMENTS

The authors would like to acknowledge USGS EROS Hazards Data Distribution System (HDDS) for providing the data.

REFERENCES

Barckley H. L. (2012) Review of liquefaction hazard information in eastern Canterbury, including Christchurch City and parts of Selwyn, Waimakariri and Hurrunui Districts. *Environment Canterbury Regional Council Report R*12/83*. GNS Science, Wellington*. 99p.

Berk, A., Bernstein, L.S., Anderson, G.P., Acharya, P.K., Robertson, D.C., Chetwynd, J.H., Adler-Golden, S.M. (1998) MODTRAN cloud and multiple scattering upgrades with application to AVIRIS. *Remote Sensing of Environment*, 65(3): pp. 367-375.

Chavez P.S. (1988) An improved Dark-Object Subtraction technique for atmospheric scattering correction of multispectral data. *Remote Sensing of Environment*, 24(3): pp. 459-479.

Chavez P.S. (1996) Image-Based Atmospheric Corrections – Revisited and Improved. *Photogrammetric Engineering & Remote Sensing*, 62(9): pp. 1025-1036.

Gebreslasie M.T., Ahmed F.B., J. van Aardt (2009) Image-based reflectance conversion of ASTER and IKONOS imagery as precursor to structural assessment of plantation forests in KwaZulu-Natal, South Africa. *Southern Forests 2009*, 71(4): pp. 259-265.

Mahiny A.S., Turner B.T. (2007) A Comparison of Four Common Atmospheric Correction Methods. *Photogrammetric Engineering & Remote Sensing*, American Society for Photogrammetry and Remote Sensing, Flagstaff, 73(4): pp. 361-368.

Mitomi, H., Matsuoka, M., Yamazaki, F., Taniguchi, H. and Ogawa, Y. (2002) Determination of the areas with building damage due to the 1995 Kobe earthquake using airborne MSS images. *Ed. IEEE International Geoscience and Remote Sensing Symposium 2002, IGARSS '02*. pp. 2871-2873.

Oommen T., Baise L.G., Gens R., Prakash A., Gupta R.P. (2010) Documenting Liquefaction Failures Using Satellite Remote Sensing. *8th International Workshop on Remote Sensing for Disaster Management*, Tokyo, Japan, 30 Sep – 1 Oct, pp. 1-10.

Ramakrishnan D., Mohanty K.K., Nayak S.R., Vinu Chandran R. (2006) Mapping liquefaction induced soil moisture changes using remote sensing technique: an attempt to map the earthquake induced liquefaction around Bhuj, Gujarat, India. *Geotechnical and Geological Engineering*, Springer Press, 24: pp. 1581-1602.

Richter R. (1996) A spatially adaptive fast atmospheric correction algorithm. *International Journal of Remote Sensing*, 17(6): pp. 1201-1214.

Richter R. (1997) Correction of atmospheric and topographic effects for high spatial resolution satellite imagery. *International Journal of Remote Sensing*, 18(5): pp. 1099-1111.

Liang S., Hongliang, F. and Mingzhen, C. (2001) Atmospheric correction of Landsat ETM+ land surface imagery. I. Methods. *IEEE Transactions on Geoscience and Remote Sensing*, 39(11):pp. 2490-2498.

Wu J., Wang D., Bauer M.E. (2005) Image-based atmospheric correction of QuickBird imagery of Minnesota cropland. *Remote Sensing of Environment* 99: pp. 315-325.

Yusuf Y., Matsuoka, M. and Yamazaki, F. (2001) Damage detection from Landsat-7 satellite for the 2001 Gujrat, India Earthquake. *Ed. 22nd Asian Conference on Remote Sensing 2001*, pp. 300-305.